INSTRUMENTATION AND EXPERIMENTAL SETUP

Gunnar Jeschke

Max Planck Institute for Polymer Research,
Mainz, Germany

Instrumentation aspects of ESR spectroscopy are treated thoroughly in a standard text (Poole 1997). However, a majority of ESR users are nowadays concerned with application work rather than development of instrumentation and methods. For such work, a comprehensive knowledge of instrumentation aspects is not required, yet a basic knowledge is needed to measure high-quality spectra and notice problems with hardware. The present chapter intends to present just this basic knowledge and to relate it to proper procedures for experimental setup. It complements Poole's book, and where more detailed descriptions are needed, they can probably be found there. For pulsed ESR and ENDOR, selected original papers on instrumentation are cited to take modern developments into account. High-field ESR beyond frequencies of 95 GHz, where no fully fledged commercial spectrometers exist, is not included here. This reflects my lack of experience rather than a judgment on the usefulness of higher frequencies for work on biological membranes and membrane proteins. Note also that I discuss instrumentation and setup procedures with particular emphasis on measuring spectra of nitroxide spin probes and spin labels, although it should not be too difficult to adapt the procedures to work on transition metal centers.

The chapter starts with a short section on continuous-wave (CW) ESR, as I feel that the physical intricacies of this experiment are often underestimated. This section also introduces basic knowledge on resonators and coupling and should be studied even if one is mainly concerned with pulsed ESR. The following section on basic pulsed ESR emphasizes the different optimization criteria for resonators compared to CW ESR and their different handling. It also discusses the question of proper echo integration, as sensitivity depends critically on the choice of the integration window. The section on pulsed ENDOR discusses the reasons for baseline problems and the fact that Davies ENDOR is better suited for large couplings and Mims ENDOR for small couplings. It also looks at the question of how to measure very small intramolecular hyperfine couplings that can provide distance information on a length scale between 0.3 and 1 nm. The final section on pulsed ELDOR stresses the fact that instrumentation for implementing ELDOR for pulsed

work is actually simpler than for CW work. The discussion of experimental setup concentrates on distance measurements. Obtaining the full information from such measurements — reliably — depends more strongly on a precise setup than is the case for most other ESR measurements.

Readers should realize that it is impossible to give foolproof setup procedures that will work with any given spectrometer. When reading this chapter, they should aim to understand *why* these particular procedures are recommended, as such understanding is the basis for adapting them to different hardware. Finally, note that references are selected merely to illustrate thoughts that cannot be evolved in detail here. They are not comprehensive, as in a review, and are not intended to provide an overview of the history of ESR instrumentation.

1. CONTINUOUS-WAVE ESR

CW ESR (Weil et al. 1994) spectra are often analyzed for their line shape or fitted by least-square procedures. This is particularly true for spectra of nitroxide spin probes or labels. Such data analysis depends crucially on how reliable the experimental line shapes are. Investing ten minutes more in a careful experimental setup may save hours of work in data analysis.

1.1. How the Signal Arises

In the CW ESR experiment the first derivative of a field-swept ESR absorption spectrum is measured. The microwave frequency $\omega_{mw} = 2\pi\,\nu_{mw}$ during the experiment is constant. Thus sensitivity can be increased by optimizing the high-frequency components for a narrow frequency band and by placing the sample in a microwave (m.w.) resonator. The use of a suitable m.w. resonator and its proper coupling are crucial for obtaining correct CW ESR line shapes. An important characteristic of the resonator (or cavity) is its loaded quality factor:

$$Q_L = \frac{\omega_{mw} L}{R_0 n^2 + r}\,, \tag{1}$$

where L is the inductivity of the resonator, R_0 is the impedance of the line that transmits the m.w. power from the source to the resonator (usually 50 Ω), n is a parameter that characterizes the coupling between transmission line and resonator, and r is the impedance of the resonator. The impedance r varies between samples due to dielectric m.w. losses in the samples. It does not include the resonant m.w. absorption of the electron spins. The quality factor is related to the width $\Delta\nu$ of the resonator mode by

$$\Delta\nu = \frac{\nu_{mw}}{Q_L}\,. \tag{2}$$
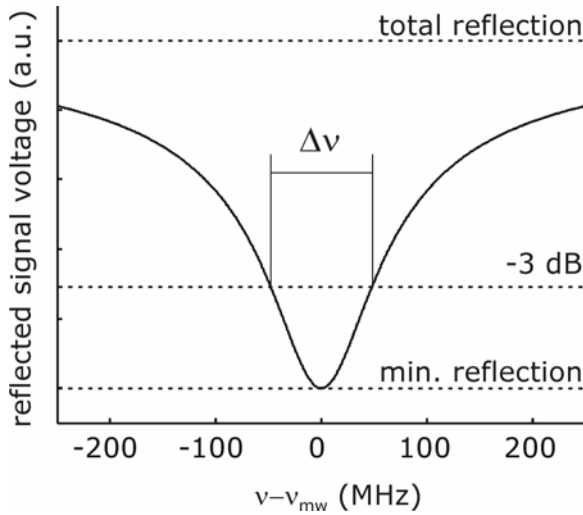
Figure 1. Idealized m.w. mode (dip) with $Q_L = 100$ at a frequency of 9.6 GHz. At the 3-dB points, the power that enters the resonator is half as large as on resonance ($\nu - \nu_{mw} = 0$). The 3-dB resonance band width $\Delta\nu$ in this example is 96 MHz.

The shape of the resonator mode is shown in Figure 1. Most CW ESR spectrometers use a reflection resonator (Figure 2). The m.w. power is transmitted through ports 1 and 2 of a circulator to the resonator and reflected power is transmitted from the resonator through ports 2 and 3 of the circulator to the detector (m.w. diode). With the electron spins off resonance, the reflected power should be zero. This is achieved by critical coupling of the resonator, i.e., the coupling is adjusted so that the condition

$$R_0 n^2 = r \tag{3}$$

is fulfilled. In this situation, all m.w. power that enters the resonator is converted to heat in the impedance r.

Now consider what happens during the field sweep when the electron spins become resonant with the irradiated m.w. frequency. The sample will then absorb additional m.w. power, which drives the ESR transition and is eventually also converted to heat via spin–lattice relaxation. In other words, the impedance of the resonator increases to $r + \Delta r$. This means that the condition of critical coupling, Eq. (3), is no longer fulfilled. Hence power is reflected from the resonator and transmitted to the detector.

Based on these considerations the dependence of the detected signal on Δr and hence on the amplitude $\chi''(\omega)$ in an ESR absorption spectrum can be derived (Feher 1957). The change in input voltage of the detector, ΔV_{refl}, is given by

$$\Delta V_{refl} = C\chi''(\omega)\eta Q_L \,, \tag{4}$$
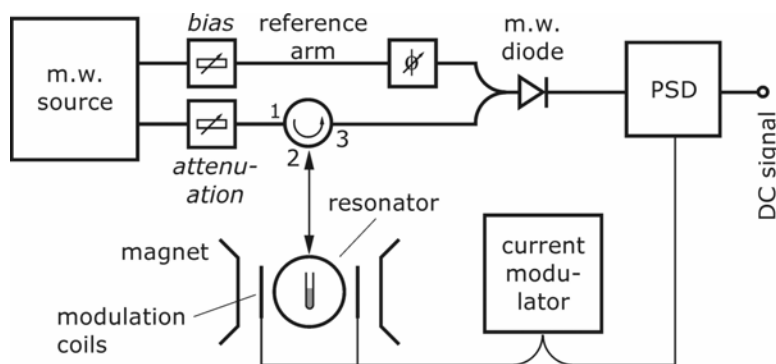
Figure 2. Simplified scheme of a CW ESR spectrometer.

where C is an instrumental constant and η is the filling factor of the resonator. The filling factor is the integral of the m.w. field amplitude B_1 over the sample volume divided by the integral of B_1 over the whole resonator.

It follows that sensitivity decreases if Q_L decreases due to dielectric losses. This is usually an important consideration in work on biological membranes or membrane proteins, since these samples contain water which has significant dielectric m.w. losses at all relevant ESR frequencies. As the dielectric losses are associated with the m.w. electric field, a good resonator should exclude the electric field from the sample volume. Furthermore, the part of the cavity where the m.w. magnetic field B_1 is concentrated should be filled as much as possible with sample. In a rectangular cavity, both these conditions can be fulfilled by placing the sample in a flat cell or in a bundle of capillaries such as a Bruker's AquaX cell. A disadvantage of flat cells and AquaX for work with precious membrane protein samples is the relatively large required sample volume. Loop-gap resonators, as available from Jagmar (Krakow, Poland) or in the U.S. via Molecular Specialties Inc. (Milwaukee, WI), have a lower intrinsic Q_L than cavities but very high η and allow for measurements with less than 1 µL of sample.

The reflected signal is usually detected by an m.w. diode (crystal detector). To measure correct line shapes the output signal of the diode needs to be linear to input voltage, i.e., to the square root of microwave power P_{mw}. At very low input power this is not the case. In order to detect the very small reflected power in the linear regime of the diode, it has to be biased by some reference power (Figure 2). Best results are achieved with a bias that puts the off-resonance detector current to 200 µA. Note that m.w. diodes are slowly destroyed by too much input power. One should avoid situations where the diode current is at the upper limit or exceeds it. Therefore, one should not touch the sample when in operate mode (this may shift the m.w. dip and lead to total reflection of the power) and decrease m.w. attenuation only gradually, as a large fraction of power may be reflected unless the resona-

tor is critically coupled. Modern spectrometers may have protection circuitry that limits the input power of the diode. However, it is good practice not to rely on such protection.
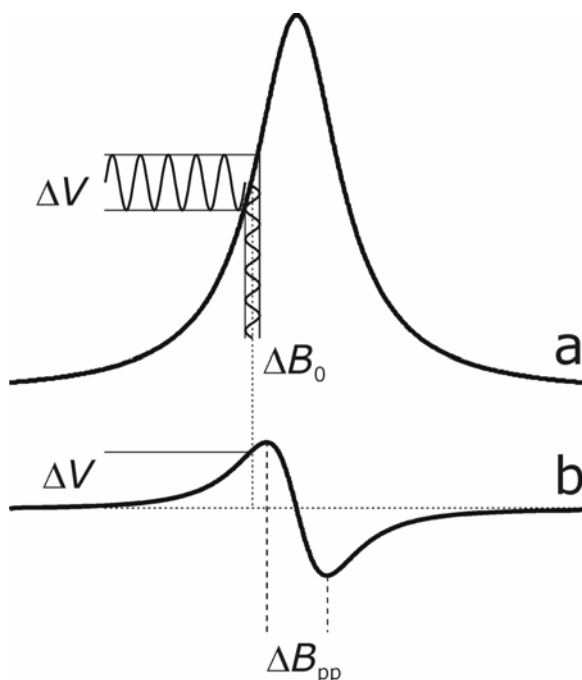
Figure 3. Detection of the first derivative of the absorption line by field modulation with amplitude ΔB_0. The signal after the m.w. diode (see Figure 2) oscillates with the frequency of the field modulation and with amplitude ΔV. The signal after the phase-sensitive detector (PSD) is a DC signal with amplitude ΔV. The field difference between the inflexion points of the absorption line is the peak-to-peak line width, ΔB_{pp}.

If one would just apply continuous m.w. power to the sample and sweep the field as described so far, the output current of the diode would be proportional to the absorption spectrum, not its derivative. The derivative is obtained by modulating the external magnetic field B_0, which leads to an oscillating absorption signal, and by detecting the amplitude of this oscillation with a phase-sensitive detector (PSD). The principle is depicted in Figure 3. The advantages of this additional step are a rejection of noise that does not oscillate with the modulation frequency and of non-resonant m.w. absorption that does not depend on the magnetic field. Furthermore, the derivative spectrum is better resolved than the absorption spectrum. As a disadvantage, signals that are much broader than the maximum modulation amplitude are hard to detect, because field modulation then causes only very small signal oscillations.

Generally, sensitivity increases with increasing modulation amplitude ΔB_0 as long as it does not exceed the line width. To obtain a very high-quality line shape for a strong sample, the amplitude of the field modulation should be five times smaller than the peak-to-peak line width, ΔB_{pp}. However, unless very small effects are to be detected in line shape analysis, the modulation amplitude can be selected as large as $\Delta B_{pp}/3$. If just the resonance field, but not the line width, is to be measured, the best sensitivity is obtained when ΔB_0 matches ΔB_{pp}. In Figure 3, the modulation amplitude was chosen 4.12 times smaller than the line width. For nitroxides, modulation amplitudes of 2 G in the solid state and 1 G in solution are usually a good choice. Two times smaller modulation amplitudes may be required for deuterated nitroxides or nitroxides that don't have protons, such as Fremy's salt. At high field, a modulation amplitude of 2 G is often tolerable even in solution.

The standard modulation frequency of 100 kHz may lead to line shape distortions by modulation sidebands for lines that are narrower than approximately 100 mG (Weil et al. 1994). Such narrow lines are hardly ever encountered with nitroxides. At high fields, it may nevertheless be advantageous to decrease the modulation frequency. This is because mechanical vibration caused by the field modulation (microphonics) can be a significant source of noise for the small and delicate high-frequency resonators. The optimum modulation frequency depends on the particular probe head and has to be found out experimentally.

1.2. Matching and Phasing with Automatic Frequency Control

Standard CW ESR spectrometers at frequencies up to Q band (35 GHz) feature automatic frequency control (AFC). By AFC small frequency shifts of the resonator mode due to temperature changes and due to the real part of the magnetic susceptibility of the sample $\chi'(\omega)$ are compensated for by automatic adjustment of the m.w. frequency. To measure with an almost critically coupled resonator, AFC is mandatory, as otherwise the magnetic susceptibility of the sample may carry the resonator from undercoupling to overcoupling (or vice versa), which leads to a sign change of the signal (Feher 1957). This effect can indeed be observed with very strong samples such as DPPH whose susceptibility upsets AFC. Adjustment of the m.w. phase is also simplified by AFC, as it keeps the frequency exactly at the center of the m.w. mode. If the mode is symmetric, as is usually the case for critically coupled resonators in this frequency range, the following procedure avoids any line shape distortions by phase errors or by nonlinear detection.

1. Go to tune mode. Switch reference arm off or set bias to zero. Find the resonator dip (m.w. mode) and shift it to the center of the display/oscilloscope picture. Adjust coupling so that the dip is as deep as possible. This is critical coupling to zeroth approximation.

2. Go to operate mode; set attenuation to 20 dB. If the diode current is at the upper limit, increase attenuation until it is in the range of the display. Adjust frequency so that AFC error is close to zero (lock offset display). Adjust coupling so that the diode current is as small as possible. *Slowly* decrease attenuation and readjust coupling, keeping diode current as small as possible. If you use the correct

sample cell and it is correctly placed in the resonator, it should be possible to decrease attenuation to 0 dB and still have the diode current at the lower limit. If you cannot get diode current to the lower limit at 20 dB, you should consider using a different sample cell or at least a tube with a smaller diameter. As a stopgap solution, you may go back to tune mode and pull the sample tube out until the dip is sufficiently narrow and deep, the restart at step 1. In fact, with resonators that are coupled from the bottom, such as in a Bruker's W-band spectrometer, pulling out the sample a bit may be a fairly efficient strategy. Once you have attained a small diode current at low m.w. attenuation, you have achieved critical coupling to first approximation. It is only a first approximation since the diode is rather insensitive at low input power.

3. Go back to 20-dB attenuation and tune mode. Switch on the reference arm and increase bias until you see significant changes in the displayed dip. Adjust phase so that the dip is as deep as possible and symmetric. Go back to operate mode and adjust AFC offset (lock offset) to zero. Adjust the bias so that the diode current is 200 µA (center of the display). Now finely adjust the phase so that the diode current is maximum. If you did everything right until here, the maximum should be only slightly above 200 µA. Readjust bias (attenuation of the reference arm) so that the diode current is again 200 µA. Note that this is a fine adjustment of phase that requires that you are already close to the correct phase. There are two phase settings where the diode current is maximum, corresponding to constructive and destructive interference of reflected and bias power. You need constructive interference, i.e., a deep dip in the tuning mode.

4. Now slowly increase attenuation to 40 dB, adjusting AFC offset if necessary. If phase and bias are correct, AFC should stay in the lock at 40 dB. Readjust bias to 200 µA if necessary. Slowly decrease attenuation while readjusting the coupling so that the diode current stays at 200 µA. Don't change the bias in this step. The highest power (lowest attenuation) at which the diode current is still 200 µA is the highest power at which you can measure reliable line shapes. Now go back to the attenuation at which you want to measure. If you fail with the 4th step, you may still measure a good line shape; the setting is just not absolutely perfect.

This procedure may seem tedious, but it is done easily and fast once learned. It guarantees that one can detect any problems with the sample, resonator, or spectrometer and obtain reliable line shapes under almost all circumstances. Some modern spectrometers have an autotune mode that is reliable as long as the mode is not broadened too strongly by m.w. losses of the sample. It is still useful to learn manual tuning, as autotune may not always work, particularly if specialized resonators are used.

At high frequencies or with samples that have strong dielectric m.w. losses in an imperfect resonator, it may sometimes be difficult to achieve critical coupling. If the diode current exceeds 200 µA with the reference arm switched off even at 20 dB attenuation and optimum coupling, one may want to measure with the reference arm off and the minimum attenuation that brings the diode current down to 200 µA. The diode is then biased by the m.w. power reflected from the cavity off resonance.

This way of operating an ESR spectrometer should only be used if proper tuning cannot be achieved.

1.3. Matching and Phasing without Automatic Frequency Control

High-frequency spectrometers often do not have AFC, or this AFC is rather unstable or ineffective. Without AFC, good line shapes can then only be obtained if everything else is very stable. The spectrometer electronics should be warmed up and the whole probe head should be at thermal equilibrium. It is therefore advisable to use temperature control with a stream of ambient temperature nitrogen even for room-temperature measurements. In any case, switch on the spectrometer and put in the sample at least half an hour before the intended measurement. Furthermore, it is usually difficult to adjust critical coupling with the same precision as at more conventional frequencies. In this situation, matching and phasing are better done with the following procedure.

1. Go to tune mode. Switch off reference arm or set bias to zero. Find the resonator dip (microwave mode) and shift it to the center of the display/oscilloscope picture. If you can adjust the frequency of your resonator, try to find a frequency where the mode is as symmetric as possible. Adjust coupling so that the dip is as deep as possible. This is critical coupling to zeroth approximation.

2. Go to operate mode. Adjust the frequency so that the diode current is as low as possible. This guarantees minimum reflection; the m.w. frequency is at the center of the dip. You may try to readjust coupling now, but note that this may shift the frequency of the mode. You thus have to readjust coupling and frequency together to minimize diode current.

3. Go to tune mode, switch on reference arm, and increase bias until you see changes in the dip. Adjust phase so that the dip is as deep as possible and as symmetric as possible. Go back to operate mode and adjust bias so that diode current is at 200 μA.

4. If your spectrometer has a setup scan feature, go to setup scan. Finely adjust the phase so that noise in the setup scan is minimized. If you don't have a setup scan feature, you can mimic this by doing short measurements of a baseline region of the spectrum and readjusting phase until noise is minimum.

The success of this procedure depends on symmetry and the frequency stability of the mode. Check for correct phase by integrating the spectrum after a baseline correction with a constant function. This baseline correction is required to cancel receiver offsets. If the phase is correct, the absorption spectrum obtained by integration also has a flat baseline at the zero level at its high-field end. Generally, spectra with correct phase are easy to measure at low field and hard to measure at high field. Spectra with wrong phase are difficult to fit with a least-squares procedure, so it pays to take care when performing the experiment.

1.4. Setting Receiver Gain and m.w. Power

Reliability of line shapes may also be affected by a too high receiver gain or a too large m.w. power. Too high receiver gain is easily recognized if the maxima and minima of the spectrum are cut off, but the line shape may already be compromised if the signal amplitude is close to the input limit of the analog-to-digital converter. Therefore, observe the receiver level display during the first scan of spectrum acquisition. If it comes close to the maximum or the minimum of the display, the receiver gain should be reduced. Lowering the receiver gain does not decrease sensitivity. If in doubt, measure with lower rather than higher receiver gain.

Reducing m.w. power usually does reduce sensitivity. Thus spectra should ideally be measured at the highest m.w. power at which saturation broadening is still absent. If signals are weak and spectra accumulated for a long time, it pays to adjust the power according to this criterion. Saturation broadening is absent as long as the signal amplitude still increases linearly with the m.w. field B_1, i.e., with the square root of m.w. power P_{mw}. Power is measured on the logarithmic dB scale. On this scale, 10 dB corresponds to a factor of 10, and 3 dB corresponds to roughly a factor of 2 ($\log 2 = 0.30103$). Hence, a 6-dB decrease in attenuation corresponds to an increase in m.w. power by a factor of 4. In the linear regime, signal amplitude should thus increase by a factor of 2. To find the maximum non-saturating power for nitroxides one may start at room temperature with an attenuation of 20 dB, at 80 K with 30 dB, and at 10 K with 50 dB, and then increase or decrease attenuation in steps of 6 dB. Note that above a certain m.w. power level, the noise level may no longer be dominated by detector noise but by phase noise from the source. If this is the case, increasing m.w. power no longer improves signal-to-noise ratio.

2. BASICS OF PULSED ESR

2.1. Pulsed ESR Hardware

Pulsed ESR (Schweiger and Jeschke 2001) requires higher m.w. power than CW ESR, a pulse-forming unit (PFU), and a detection technique that does not depend on field modulation (Figure 4). Usually pulses are formed at powers of less than 1 W and are amplified later. A good pulse-forming unit (PFU) allows for separate power and phase adjustments of at least two channels. For some experiments, four independent channels are required. The power level of the whole pulse sequence can be adjusted with a main attenuator. At least the main attenuator should be calibrated, i.e., it should be possible to select its attenuation on a dB scale.

Pulsed ESR experiments depend on excitation bandwidths of at least a few megahertz — often tens of megahertz. The bandwidth of a resonator is defined as the frequency difference $\Delta \nu$ between its 3-dB points, i.e., between the upper and lower frequencies where the power in the resonator is attenuated by a factor of two
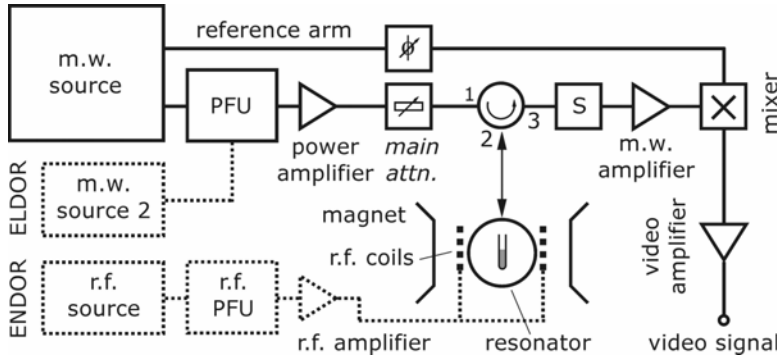
Figure 4. Simplified scheme of a pulsed ESR spectrometer. Optional components required for pulsed ELDOR or ENDOR are displayed as dashed parts.

compared to the center of the dip (Figure 1). A critically coupled high-Q resonator at X band ($Q_L \approx 5000$ or more), such as an m.w. cavity, a loop-gap resonator (Froncisz and Hyde 1982), or a dielectric resonator, has a bandwidth of less than 2 MHz according to Eq. (2). Such resonators have to be overcoupled ($R_0 n^2 > r$ in Eq. (1)). In Figure 1, overcoupling to $Q_L = 100$ is assumed, so that $\Delta\nu = 96$ MHz at $\nu_{mw} = 9.6$ GHz. At such low Q_L values, cavity resonators are not competitive with other resonator types that have larger filling factors. Loop-gap, split-ring, and dielectric resonators are well suited and similar to each other in performance. For resonators with intrinsically low Q_L, such as the bridged loop-gap resonator (Pfenninger et al. 1988), Q_L can be adjusted only within a small range. As finding the correct dip requires at least moderate Q_L and the measurements require small Q_L, such resonators may be more difficult to work with. Nevertheless, they are valuable for special applications where their transparency to radio frequency (r.f.) fields is important (Schweiger and Jeschke 2001).

The bandwidth of the resonator also influences the shape of the m.w. pulses, and thus the dead time t_d that passes after a pulse before the signal can be detected. In an ideal resonance circuit, signals rise as $1 - \exp(-t/\tau)$ and fall as $\exp(-t/\tau)$ (see inset in Figure 5b). The rise time τ is related to Q_L by

$$\tau = \frac{Q_L}{\pi\nu_{mw}}, \tag{5}$$

corresponding to $\tau = 3.3$ ns for $Q_L = 100$ at $\nu_{mw} = 9.6$ GHz. The actual dead time depends on pulse power P_{mw} and signal power P_{signal}, as at the time of detection the pulse power (ringing) should have decayed to a level significantly lower than P_{signal}. For the power of a 1-kW m.w. pulse to decay to less than 1 µW, the dead time in the above example would be $t_d = 68$ ns. The actual dead time can never be shorter than the one imposed by the bandwidth of the resonator, but it can be longer if m.w. power is reflected forth and back in transmission lines.
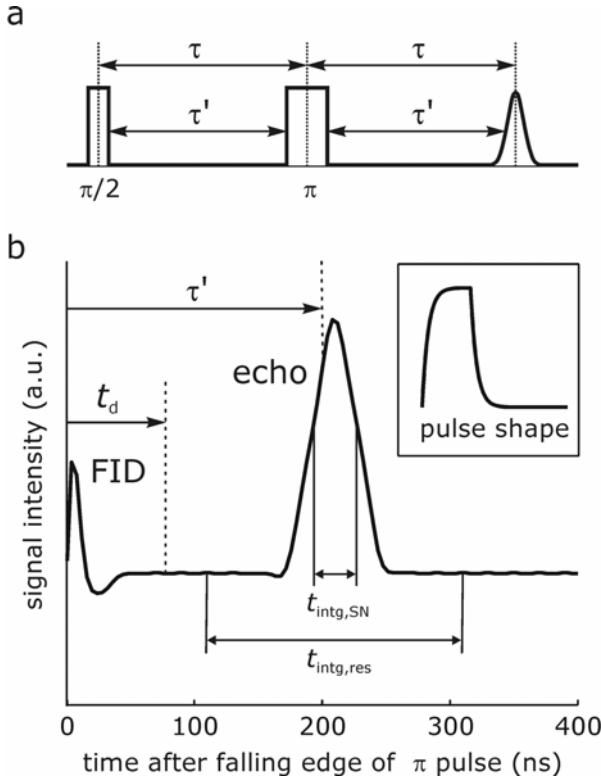
Figure 5. Precise definition of interpulse delays τ in echo sequences (a) and optimum integration windows (b) for reasonable field resolution in echo-detected field-swept EPR ($t_{intg,res}$ = 200 ns) and for maximum sensitivity in non-selective experiments such as ESEEM, ENDOR, or DEER ($t_{intg,SN}$ = 32 ns). The signal trace is a simulation for a two-pulse echo sequence with $t_{\pi/2}$ = 16 ns, t_π = 32 ns, τ' = 200 ns (τ = 224 ns) applied to a Gaussian ESR line with a full width at half height of 84 MHz (30 G). The inset in (b) shows the shape of a pulse with a length of 32 ns assuming rise and fall times of 4 ns.

To obtain maximum detection sensitivity and maximum m.w. field strength B_1 at given m.w. power P_{mw}, Q_L should not be lowered unnecessarily. The field strength is given by

$$B_1 = \sqrt{\frac{2\mu_0 Q_L P_{mw}}{V_c \nu_{mw}}},$$ (6)

where V_c is the effective volume of the resonator. The field strength is related to duration t_p and flip angle β of the pulse by

$$\beta = F \frac{g\mu_B B_1}{\hbar} t_p,$$ (7)

where $F = 1$ for species with electron spin $S = 1/2$ and

$$F = \sqrt{S(S+1) - m_S(m_S + 1)},\tag{8}$$

if the pulse drives a single transition of spin $S > 1/2$ between the states with magnetic quantum numbers m_S and $m_S + 1$. If the pulse excites all transitions of a spin $S > 1/2$ simultaneously, $F = 1$.

Short pulses are necessary to achieve large excitation bandwidths,

$$\Delta\nu_{exc} \approx \frac{1.2}{t_p},\tag{9}$$

and to avoid significant relaxation of the electron spins during the pulse. Here the excitation bandwidth $\Delta\nu_{exc}$ is defined by the full width at half height of the theoretical excitation profile of a rectangular pulse. A pulse with a width of 12 ns thus has an excitation bandwidth of ± 50 MHz. Since 2.8 MHz corresponds to 1 G at $g = g_e$, the excitation bandwidth on a field scale is ± 18 G. According to Eq. (7), such an excitation bandwidth requires $B_1 = 93$ G in our X-band example for a pulse with $\beta = \pi$.

From Eq. (6) it becomes clear that at given m.w. power a larger B_1 can be achieved with a smaller active volume V_c of the resonator. Using such a smaller resonator does not lead to a decrease of concentration sensitivity as long as the filling factor η can be maintained. In practice, miniaturization of resonators tends to decrease η somewhat as the ratio of wall thickness of the sample tube to resonator dimension increases. However, in work with membrane proteins absolute sensitivity is often more important as the amount of sample is limited. Absolute sensitivity increases with decreasing resonator size. If the filling factor remains the same, absolute sensitivity is approximately proportional to the inverse third power of the resonator dimension. In practice, the filling factor decreases somewhat with resonator size as sample container walls cannot be made proportionally thinner.

Working with overcoupled resonators has the disadvantage that much of the power is reflected. Even if pulses are short and duty cycles low, a reflected power of some hundred watts would damage any detector that is sensitive enough to measure signals that have only microwatts of power. Hence, the detection circuitry has to be protected either by a switch (S in Figure 4) or by a power limiter. A switch has to be closed well before high-power pulses are applied and has to remain closed until the pulse power has decayed down to the milliwatt level. This is usually done by control software and an auxiliary pulse from the pulse pattern generator. It is good practice to keep the main attenuator at 60 dB until the presence of the protection window in the signal trace has been verified by an oscilloscope or in a Bruker's SpectJet window.

In pulsed ESR spectrometers signals are detected by downconversion to video frequencies (between zero and 100 MHz) with a mixer. A mixer combines m.w. directly from the source (transmitted through the reference arm) with the m.w. coming from the sample. Video output is at the difference frequency. Such down-

conversion by a mixer causes a significant loss in signal-to-noise ratio if one of the input signals would have an amplitude below the noise level of the mixer. Therefore the m.w. coming from the sample needs to be pre-amplified (see Figure 4). The m.w. pre-amplifier usually has a fixed gain. Signal amplitude can be varied by changing the gain of the video amplifier that follows after the mixer. Video amplifier gain should be adjusted so that the maximum signal during the experiment is about 1/2 to 2/3 of the maximum input of the analog-to-digital converter. In rare cases the signal already saturates the m.w. pre-amplifier. Even with the lowest gain of the video amplifier one then observes an echo that appears flattened at the top or line shape distortions in echo-detected ESR spectra (a "compressed" top or even a cutoff near the maximum). For such strong signals the m.w. pre-amplifier has to be switched off.

2.2. Adjusting Pulse Amplitude and Phase

Before setting up a pulse ESR experiment one decides on the desired excitation bandwidths and hence lengths of all the pulses. For nitroxide spin labels the maximum feasible excitation bandwidth is smaller than the total width of the spectrum. The excitation bandwidth of the longest pulse in the sequence then decides what fraction of the spins contributes to the signal. Hence, sensitivity increases with decreasing duration of the longest pulse. On most spectrometers the rise time of the m.w. switches and the minimum Q_L of the resonator do not allow for well-defined pulses shorter than 8 ns. Depending on the resonator and the available m.w. power, the minimum length of a pulse with flip angle $\pi/2$ or π according to Eqs. (6) and (7) may be even longer. Experience tells what is feasible with a given spectrometer and probe head. If one decides that π pulses have twice the length of $\pi/2$ pulses, one can use the same pulse channel for both of them. In HYSCORE (Höfer et al. 1986) and PELDOR or DEER (Milov et al. 1984; Pannier et al. 2000) experiments, it is advisable that the π pulses have the same length as the $\pi/2$ pulses, so that different channels with separately adjustable power are required.

The number of required channels also depends on phase cycling (Schweiger and Jeschke 2001). In most ESR pulse sequences at most two phases ($+x$ and $-x$) will suffice for any given pulse. Single-frequency experiments for distance measurements such as double-quantum techniques (Borbat and Freed 2000) or the SIFTER experiment (Jeschke et al. 2000) require four phases ($+x$, $+y$, $-x$, $-y$) for certain pulses. In recent Bruker bridges (stripline bridges) there are preset channels for these four phases, which simplifies setup. Note, however, that such preset channels are optimized at a certain m.w. frequency. Depending on probe head and sample properties (dielectric permittivity) one may be forced to perform measurements at a frequency where the preset phases are slightly off. The following procedures, and pulse experiments on nitroxides in general, work well in the temperature range between 50 and 80 K. Lower temperatures lead to an increase in T_1 that forces slower repetition of the experiment without leading to an increase in T_2. At higher temperatures, T_2 may drop strongly in some matrices (e.g., glassy ethanol),

so that a significant part of the signal is lost by relaxation. Generally, pulse ESR on nitroxides is feasible up to temperatures 10 K below the glass transition temperature of the matrix.

The first step in experiment planning is thus to decide which pulse length/flip angle/phase combinations are required to perform the experiment and to assign these combinations to the available pulse channels. After that the proper power level and phase for all those channels have to be set. Spectrometer electronics and the probe head should be in thermal equilibrium at that time, i.e., the probe head should have been cooled down to the target temperature and the spectrometer switched on 30 minutes before setup. For relatively short pulses up to 200 ns length setup is most easily done with an echo sequence: pulse(t_p)–delay(τ)–pulse($2t_p$)–delay(τ)–echo for $\pi/2$ pulses with length t_p and with a sequence: pulse($t_{p/2}$)–delay(τ)–pulse(t_p)–delay(τ)–echo for π pulses with length t_p. For channels with preset phases and no individual attenuators, power has to be adjusted with the main attenuator. If the channels have individual attenuators, it is advisable to set the main attenuator to 0 dB and to adjust pulse power with the channel attenuators. Before this is done, the m.w. frequency ν_{mw} should be determined and the magnetic field set to the expected maximum of the nitroxide spectrum. The maximum corresponds to $g_y \approx 2.006$, and the field can be computed by $B_0/G = 356 \, \nu_{mw}/GHz$.

The following setup procedure assumes quadrature detection, i.e., both the real and imaginary part of the signal are observed. For a $+x$ channel, start with maximum attenuation (minimum power) and slowly decrease attenuation. An echo signal with at first arbitrary phase (components in both the real and imaginary part) should appear. Next, slowly decrease the attenuation until the echo amplitude stops increasing and eventually decreases. Adjust the video gain so that the echo is clearly visible. Now adjust the signal phase, preferably by using the main phase shifter that acts on the reference arm. The signal should be in the real part and positive, as shown in Figure 5b. The signal in the imaginary part should be symmetric about zero, i.e., it should look like a dispersion line. Once the phase is correct, fine adjust the power by searching for the maximum echo amplitude. This may unbalance the phase a little bit, so that the signal phase has to be readjusted.

This procedure has to be repeated for all required channels. However, in all channels except for $+x$ the channel phase shifter is used rather than the main phase shifter for phase adjustment. A $+y$ channel should have a maximum positive echo in the *imaginary* part, a $-x$ channel maximum *negative* echo in the real part, and a $-y$ channel maximum negative echo in the imaginary part. Setup of inversion pulses for Davies ENDOR (Davies 1974) or for pulse ELDOR experiments follows a different procedure (see below).

For soft pulses longer than 200 ns, the free induction decay (FID) signal that directly follows a single pulse is longer than the dead time, even if the ESR line is infinitely broad (Schweiger and Jeschke 2001). In this case, adjustment of power and phase is better done on this FID signal. Note that the FID signal reaches its maximum amplitude at flip angle π, not $\pi/2$, if the excitation bandwidth of the pulse is much smaller than the ESR line width. Further increase of the

power does not lead to a smaller amplitude of the FID but to an easily recognizable deformation.

2.3. Echo Integration

Most pulse ESR experiments on solids use echo detection, i.e., echo intensity is recorded as a function of one or two variables, such as magnetic field, delay times in the pulse sequence, r.f in ENDOR experiments, or a second m.w. frequency in some ELDOR experiments. The echo amplitude is integrated over some window of length t_{intg}, which is at least as long as the time resolution of the detection circuit, but can be much longer. The center of the window should coincide with the echo maximum. Note that the actual delay τ between pulses is the time that passes between the *centers* of the pulses, not their edges (Figure 5a). The optimum width, t_{intg}, of the integration window depends on the type of experiment.

In recording echo intensity as a function of the magnetic field (echo-detected field-swept ESR), a too short integration window can lead to line shape distortions. The distortions result from an excitation bandwidth of the pulses that is larger than the width of the most narrow features in the absorption spectrum. As the echo amplitude (maximum intensity) in the time domain corresponds to the integral of the intensity over the whole excitation window in the frequency (or field) domain, the lines are broadened. To obtain the intensity in the frequency domain at only the resonance field, one has to integrate over the whole echo. In practice, $t_{intg} = 200$ ns suffices for nitroxides in the solid state. The window should be symmetric about the echo maximum (Figure 5b). A long integration window also helps alleviate line shape distortions that may arise for short windows due to nuclear modulation effects. For spectra with some very narrow features, a much longer integration window may be required. In this situation, symmetric placement would necessitate a very long interpulse delay τ in the echo sequence and would thus lead to relaxational losses. It is then better to work with short τ and start the integration window at the echo maximum. Note also that the echo maximum does not occur at time τ after the falling edge of the π pulse, but somewhat later (Figure 5).

In experiments other than field-swept ESR, contributions from spins in the whole excitation window are usually wanted. The integration window should then be as long as the longest m.w. pulse, as this maximizes the signal-to-noise ratio (Figures 5 and 6). If the integration window is selected four times as long as the longest pulse, one already needs six times as many accumulations to obtain the same signal-to-noise ratio.

3. PULSED ENDOR

3.1. Pulsed ENDOR Spectrometer

A basic introduction to pulsed ENDOR (Gemperle and Schweiger 1991) and more detailed descriptions of sophisticated experiments (Schweiger and Jeschke
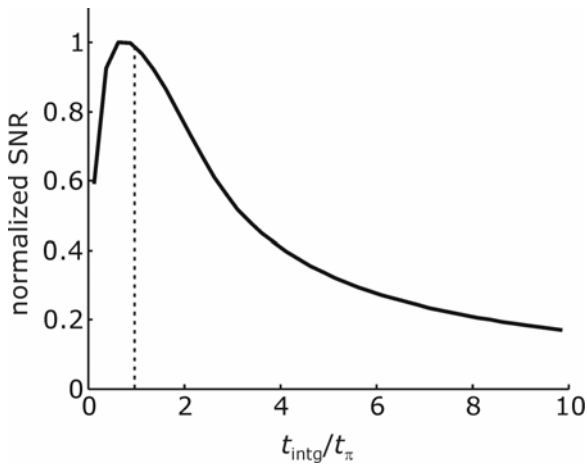
Figure 6. Normalized signal-to-noise ratio (SNR) as a function of the width, t_{intg}, of an integration window centered at the echo maximum (simulation). The simulation is the same as in Figure 5 with white noise added. The time axis is normalized to the π pulse length.

2001) can be found in the literature. To extend a pulsed ESR spectrometer to a pulsed ENDOR spectrometer, an r.f. source, a pulse former for the r.f. pulses, and a broadband high-power r.f. amplifier need to be added (see Figure 3). Furthermore, r.f. coils have to be added to the probe head. The r.f. source and amplifier should cover the range between at least 1 and 30 MHz at the X band and between 1 and 200 MHz at the W band. Typical r.f. pulse powers are a few hundred watts at pulse lengths between 1 and 200 μs with repetition times between 1 and 10 ms. In most cases the r.f. coils are terminated by a 50-Ω load. For pulses with 1 kW power and a length of 100 μs at a repetition time of 10 ms, this load must be able to withstand an average power of 10 W. The r.f. source, pulse former, and amplifier are standard devices. Performance of the pulse ENDOR spectrometer depends decisively on the design of the r.f. coils, the resonator, and on matching between the r.f. transmission line and coils.

Simply adding r.f. coils to a standard resonator does not work, since most good m.w. resonator designs feature rather massive metal walls that cannot be penetrated by r.f. The most elegant solution, at least at moderate m.w. frequencies, is to place the r.f. coil inside the resonator as close to the sample tube as possible. This can be done with a Helmholtz coil with rectangular shape (Bietsch and von Schütz 1993). Such a coil has straight wires that are parallel to the cylinder axis of a dielectric resonator. These wires do not cause a decrease in quality factor Q_L, as they do not shortcut the m.w. field.

Alternatively, the m.w. resonator can be made transparent or at least partially transparent to the r.f. field. Such approaches are based on the large difference between the m.w. and r.f. wavelengths. In most cases the m.w. frequency exceeds the

r.f. frequency by at least a factor of 680 (ratio of the resonance frequencies of electron spins with $g = g_e$ and protons). Thus, the conducting wall of a bridged loop-gap resonator (Pfenninger et al. 1988) can be made sufficiently thick to be impenetrable to m.w. fields and at the same time sufficiently thin to be transparent for r.f. fields. The r.f. coil can then be placed outside the resonator. Since such a coil has a somewhat larger volume than a coil that encloses only the sample, but not the resonator, more r.f. power is required to generate an r.f. field of the same amplitude, B_2. On the other hand, a more massive coil can be used and thermal effects on the sample or resonator are smaller at a given power. At high frequencies (95 GHz and above) the most successful design places the coil outside a TE_{011} (cylindrical) cavity that is made of ring sections connected by only a single conducting bridge (Burghaus et al. Möbius 1992). Such a cavity is almost transparent to r.f. fields (0.5 dB attenuation at 140 MHz) yet has a quality factor that is only moderately compromised with respect to a massive TE_{011} cavity.

Matching between the r.f. transmission line and the coils is achieved by a matching network consisting of capacitances and, occasionally, resistances. The design of a matching network is aimed either at broadband matching without the requirement for adjustments during an r.f. sweep or at obtaining a resonant enhancement of r.f. field B_2. In the latter case, the matching network has to be tuned to the current r.f. frequency, which can be realized by adjusting a variable capacitance by a stepper motor via a feedback loop (Forrer et al. 1990). At the same incident r.f. power, a tuned circuit achieves higher B_2 fields and thus shorter r.f. π pulses than a broadband matching network. The disadvantages are limitations in the rate of the r.f. sweep and the fact that the power is converted to heat in the coil close to the sample rather than in an external load. At high r.f. frequencies, a tunable resonant matching network requires very short coaxial feeds between the network and the coil, which is hard to realize for low-temperature measurements. Broadband matching networks contain a resistance. Considerations for a network that works well for proton ENDOR at 95 GHz m.w. frequency have been described (Rohrer et al. 1995). Reasonable broadband matching over the whole range of ENDOR frequencies at W band (2–200 MHz) is achieved in a Bruker E680 spectrometer. Matching over such a broad frequency range is not uniform, at least with long coaxial feeds between the network and coil. Combined with the thermal effects due to the proximity of the r.f. coil and the small high-frequency resonator, this leads to baseline artefacts that may be difficult to distinguish from broad ENDOR signals. These artefacts can be converted to uniform noise, and thus averaged, by varying the r.f. stochastically rather than sweeping it linearly (Epel et al. 2003).

3.2. Sensitivity Considerations on Mims and Davies ENDOR

In both established pulsed ENDOR techniques (Mims 1965; Davies 1974) sensitivity varies with the magnitude of the hyperfine coupling, A. In both cases sensitivity approaches zero if A approaches zero. In Mims ENDOR sensitivity as a function of A depends strongly on interpulse delay τ between the first two m.w. pulses

and only slightly on pulse length. In contrast, in Davies ENDOR there is no dependence on the interpulse delays but a strong dependence on the length t_{inv} of the first m.w. pulse. Except for the case where only very large couplings $A > 50$ MHz are to be detected, this implies that the first m.w. pulse in Davies ENDOR has to be longer than the pulses in Mims ENDOR. This in turn means that a smaller fraction of the spins takes part in Davies compared to Mims ENDOR experiments. The intrinsic sensitivity of Mims ENDOR should thus be higher. On the other hand, Mims ENDOR features blind spots, i.e., the ENDOR effect is almost totally suppressed at certain frequencies. For ideal (infinitely short) m.w. pulses, Mims ENDOR efficiency is given by

$$F_{\text{ENDOR}} = \frac{1}{2}\sin^2\left(A\tau\right) , \qquad (10)$$

where A is expressed in angular frequency units. As delay τ must be at least as long as dead time t_d, blind spots cannot be avoided for frequencies larger than $1/(2t_d)$. At the X band with a typical dead time of 80 ns, the first blind spot corresponds to a hyperfine coupling as small as 6.25 MHz. For m.w. pulses with finite length, suppression at the blind spots is not total, as illustrated in Figure 8, but still very pronounced. However, the comparison of Mims ENDOR with $\tau = 400$ ns (dotted line in Figure 8) and Davies ENDOR with $t_{\text{inv}} = 100$ ns (solid line) by simulations also shows that the average sensitivity is better for Mims ENDOR up to hyperfine couplings beyond the first blind spot. For very small hyperfine couplings $A < A_1$ (arrow in Figure 8), Mims ENDOR with fixed interpulse delay τ is the most sensitive experiment. For $A > A_1$, the blind spots can be almost averaged by summation of 50 Mims ENDOR experiments with τ values in the range from 100 to 492 ns (dashed line in Figure 8). This experiment is more sensitive than Mims ENDOR with fixed τ for $A > A_1$ and superior to Davies ENDOR for $A < A_2$. For larger couplings, Davies ENDOR is the most sensitive experiment.

There is one caveat about these simulations: they assume that the polarization grating generated by the first two m.w. pulses in the Mims ENDOR experiment (Schweiger and Jeschke 2001) has the same lifetime as the hole burnt by the first m.w. pulse in the Davies ENDOR experiment. As the polarization grating is a finer structure in the frequency domain, it has a shorter lifetime if spectral diffusion is significant. To decide which experiment is better for a given class of samples, one needs to quantify the influence of spectral diffusion on the stimulated echo. This can be done by comparing the decay of the echo signal as a function of interpulse delay T for the Davies observer sequence $\pi(t_{\text{inv}})$–delay(T)–$\pi/2$(16 ns)–delay(τ)–π(32 ns)–delay(τ)–$echo$ (upper sequence in Figure 7a) and the Mims observer sequence $\pi/2$(16 ns)–delay(τ)–$\pi/2$(16 ns)–delay(T)–$\pi/2$(16 ns)–delay(τ)–$echo$ (upper sequence in Figure 7b). Let $T_0 = \tau + 100$ ns (the shortest delay that does not require phase cycling), while T_{ENDOR} is the delay required for inserting the r.f. π pulse. The influence of spectral diffusion can then be quantified via the echo integrals by

$$R = \frac{V_{\text{Mims}}\left(T_{\text{ENDOR}}\right)V_{\text{Davies}}\left(T_0\right)}{V_{\text{Davies}}\left(T_{\text{ENDOR}}\right)V_{\text{Mims}}\left(T_0\right)} . \qquad (11)$$
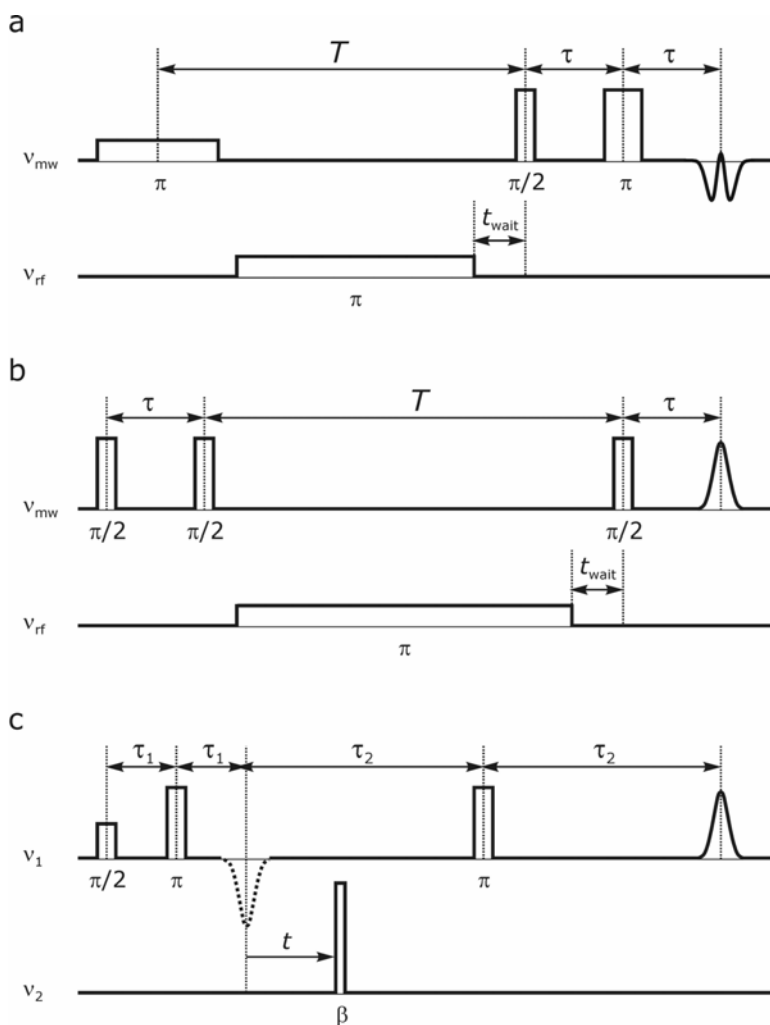
Figure 7. Pulse sequences for double resonance experiments: (a) Davies ENDOR, (b) Mims ENDOR, (c) four-pulse DEER.

A value of $R = 1$ indicates negligible spectral diffusion during an ENDOR experiment and favors Mims ENDOR, while a value of $R \ll 1$ corresponds to strong spin diffusion and favors Davies ENDOR. In fact, the functions plotted in Figure 8 for Mims ENDOR can be multiplied by R to obtain an estimate of the range of hyperfine couplings for which each experiment is advantageous. Knowing the echo decay as a function of T for the observer sequences is also useful for deciding on the optimum length of the r.f. pulse (see below).
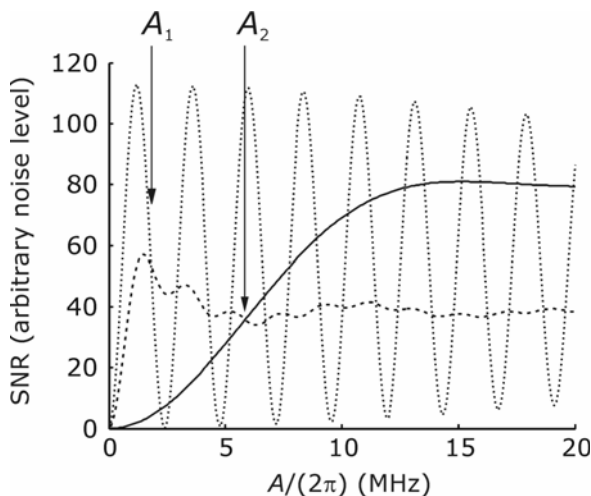
Figure 8. Signal-to-noise ratio as a function of hyperfine coupling for several pulsed ENDOR experiments at arbitrary, but common noise level (simulation, an electron phase memory time T_m of 1 μs was assumed). The same total number of accumulations and optimum integration windows for all experiments was assumed. Mims ENDOR with τ = 400 ns (dotted line) is the best experiment for $A < A_1$. Summation of 50 Mims ENDOR experiments with equidistant τ values between 100 and 492 ns (dashed line) performs best for $A_1 < A < A_2$. Davies ENDOR with a length t_{inv} = 100 ns for the first m.w. pulse (solid line) is best for $A > A_2$.

3.3. Setting up Mims ENDOR

Mims ENDOR sensitivity is optimum for the shortest π/2 m.w. pulses that are feasible on a certain spectrometer. Depending on available m.w. power and the resonator, typical values are between 8 and 24 ns at X band and between 30 and 200 ns at W band. Pulse power and phase should be adjusted for the Mims ENDOR observer sequence (upper sequence Figure 7b) rather than for a π/2–τ–π two-pulse echo. The length of the integration window should match the full width at half height of the echo. For detecting couplings between 2 and 5 MHz, the minimum feasible τ value should be used, which is typically 100–120 ns at X-band frequencies. If couplings larger than 5 MHz are expected, averaging over τ (see Figure 8) is strongly recommended. The maximum τ value in such averaging determines the sensitivity toward small couplings. A value of 500 ns should be amply sufficient in most practical cases. Notable exceptions are distance measurements by intramolecular ENDOR or other measurements of very small hyperfine couplings of rare spins. This case is discussed in §3.5.

The r.f. pulse should be a π pulse. The r.f. π pulse length for a given spectrometer, probehead, and r.f. frequency can be determined for a standard sample by a transient nuclear nutation experiment (Schweiger and Jeschke 2001). In this experiment the r.f. frequency is set to an ENDOR line of the standard sample and

kept fixed, while the length of the r.f. pulse is incremented. With a good digital oscilloscope, such as a Bruker's SpectJet, it is also possible to preselect the r.f. pulse length and adjust the power while observing changes in the echo amplitude online. Starting at a very low value, the length (or power) should be incremented until the first minimum of the echo intensity is observed. These adjustments work best with single crystals as standard samples. For measurements between room temperature and 80 K, γ-irradiated crystals of α-glucopyranoside or malonic acid are well suited. For measurements at temperatures between 4 and 20 K, glycine doped with 1% $CuCl_2$ is a good standard sample. When using powder samples or frozen solutions, one often observes only a saturation of the ENDOR effect with increasing pulse length or power rather than an oscillatory behavior. A typical length of an r.f. π pulse with broadband matching is 10 μs at proton frequencies in both X-band and W-band ENDOR. With a resonant (tuned) circuit, pulse lengths as short as 2 μs can be obtained. However, short r.f. pulses cause power broadening of the ENDOR lines and may thus decrease resolution. To obtain the resolution of 100 kHz that is usually feasible in proton ENDOR, the r.f. π pulse should not be shorter than 10 μs. For rare spins, such as ^{31}P or ^{14}N, intrinsic line widths can be significantly lower than 100 kHz. An r.f. pulse length of 40 μs is then recommended unless this leads to strong sensitivity loss due to spectral diffusion (see §3.2).

The rising edge of the r.f. pulse must be timed well after the second m.w. pulse of the observer sequence (see Figure 7b). An overlap is recognized easily by an echo suppression that occurs even if the r.f. is off resonance. After the falling edge of the r.f. pulse, a time $t_{wait} > 1$ μs should pass before the final m.w. observer pulse is applied (Figure 7b). Ringing of the r.f. pulse, in particular at low frequencies, may otherwise distort the baseline.

High-power r.f. amplifiers usually generate 3rd and 5th harmonics of the amplified frequency when they are operated at maximum output power. Indeed, the matching network may generate such harmonics even if they are not present in the r.f. that comes from the amplifier. In ENDOR spectra, harmonics manifest themselves by ghost signals at 1/3 or 1/5 of the true ENDOR frequencies. In particular, proton ghost signals are frequently encountered. For heteronuclear ENDOR, it is therefore advisable to use a low-pass filter with a cutoff frequency of 10 MHz for X-band work and 100 MHz for W-band work. The filter must be connected directly to the probe head, even if this somewhat compromises the efficiency of the matching network.

3.4. Setting up Davies ENDOR

The fraction of spins taking part in a Davies ENDOR experiment is determined by the length t_{inv} of the first observer pulse (inversion pulse). This length should be 100 ns or shorter; if a longer inversion pulse is needed to see the hyperfine couplings desired, it would be best to measure Mims ENDOR. The spins taking part in the experiment should be detected as completely as possible, i.e., the

observer echo should be formed with the shortest $\pi/2$ and π pulses that can be generated. The observer echo shape then looks as in Figure 9: a narrow positive echo superimposed by a broad inverted echo. The narrow positive echo does not exhibit an ENDOR effect. Therefore, maximum Davies ENDOR sensitivity is obtained for an integration window that matches the length t_{inv} of the inversion pulse and thus the width of the inverted echo (see Figure 9). Simulations show that this is true irrespective of the magnitude of the hyperfine coupling.
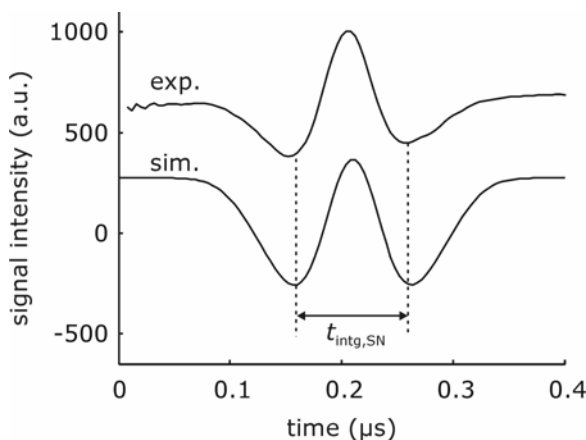
Figure 9. Experimental (upper trace, coffee) and simulated (lower trace, Gaussian line with 7-G full width at half height) signal for a Davies-ENDOR observer sequence $\beta(100 \text{ ns})$ – delay (12 μs) – $\pi/2$ (16 ns) – delay (400 ns) – π (32 ns) – delay (200 ns) and optimum width t_{intg} of the integration window.

Setup starts with optimizing the power and phase for the final two m.w. pulses by maximizing the narrow positive echo. In this step the inversion pulse channel is at maximum attenuation (minimum power). Then the power of the inversion pulse is adjusted by searching for a maximum negative broad echo. Note that the phase of the inversion pulse does not matter.

Considerations on the power and duration of the r.f. pulse as well as on its timing are the same as for Mims ENDOR. Note that adjustment of r.f. power by online echo observation is done more easily and more precisely by Mims ENDOR.

3.5. Distance Measurements by ENDOR

Intermolecular hyperfine couplings are usually strongly dominated by the dipole–dipole interaction between electron and nuclear spins. Relevant exceptions are protons of neighboring molecules that are hydrogen-bonded to the paramagnetic molecule and ^{19}F nuclei, which have substantial isotropic hyperfine couplings for very small spin densities. If the dipole–dipole interaction dominates, distance measurements in supramolecular assemblies such as biomembranes are feasible, as

this interaction is inversely proportional to the cube of the distance between the spins. The distance range depends critically on the ability to measure very small hyperfine couplings. According to Eq. (10), the measurement of small couplings requires a long interpulse delay τ in Mims ENDOR. However, the intensity of the observer echo decreases with increasing τ due to electron spin relaxation. It can be shown that in the limit of small couplings, maximum sensitivity is obtained at $\tau = T_m$, where T_m is the phase memory time of the electron spins (Zänker et al. 2004). More precisely, in that context T_m is the decay time of a stimulated echo with respect to τ. This decay time may depend on interpulse delay T between the second and third pulses, as spectral diffusion during that time contributes to the decay.

Due to this dependence on spectral diffusion, T_m strongly varies with the matrix. Typical values for $T = 12$ µs are between 800 and 1000 ns at a temperature of 80 K, but in some membrane protein preparations we have found values as short as 400 ns. As T_m decreases with increasing delay T, the sensitivity of the experiment may decrease significantly when the r.f. π pulse is prolonged. For electron spin ^{31}P distances of up to 1 nm in phospholipids in solution, a pulse length of 40 µs was found to be optimal (Zänker et al. 2004). Measurements with this pulse length are also feasible in phospholipid bilayers both at X- and W-band frequencies. The technique can be used to determine the distance of closest approach of a spin label to the layer of phospholipid head groups.

4. PULSED ELDOR (DEER)

4.1. Pulsed ELDOR Spectrometer

Extending a pulsed ESR spectrometer to a pulsed ELDOR spectrometer is less elaborate than extending a CW ESR spectrometer to ELDOR operation or a pulsed ESR spectrometer to ENDOR operation. For pulsed ELDOR, the same probe heads and the same high-power amplifier can be used as for basic pulse ESR. If a spare pulse channel is available, the same pulse-forming unit can be used as well. The m.w. power from a second source with adjustable frequency can then be fed in as input into one channel of the m.w. pulse-forming unit (see Figure 4). The same is true for high-frequency spectrometers with a design in which pulses are formed at a relatively low microwave frequency and the high frequency is obtained by several steps of frequency doubling or by mixing with continuous-wave high frequency (upconversion). In these designs, only a second source for the low frequency has to be added. Such instrumentation is sufficient for high-quality distance measurements by pulsed ELDOR techniques, if the four-pulse double electron electron resonance (DEER) sequence (Pannier et al. 2000) is applied. With a more elaborate setup, using a bimodal resonator and separate high-power amplifiers for the two m.w. frequencies (Milov et al. 1998), the more simple three-pulse sequence (Milov et al. 1984) can also provide essentially dead-time-free high-quality data. Note, however, that in a setup with a bimodal resonator the difference of the two m.w. frequencies is essentially fixed and cannot be adapted to the problem at hand. For

experiments such as two-frequency soft ESEEM, a phase lock between the two frequencies has to be implemented (Schweiger et al. 1990). However, for pulsed ELDOR distance measurements a phase lock is detrimental, as echoes between the pump pulse and observer pulses would then add up during signal accumulation. They cancel if the sources are incoherent.
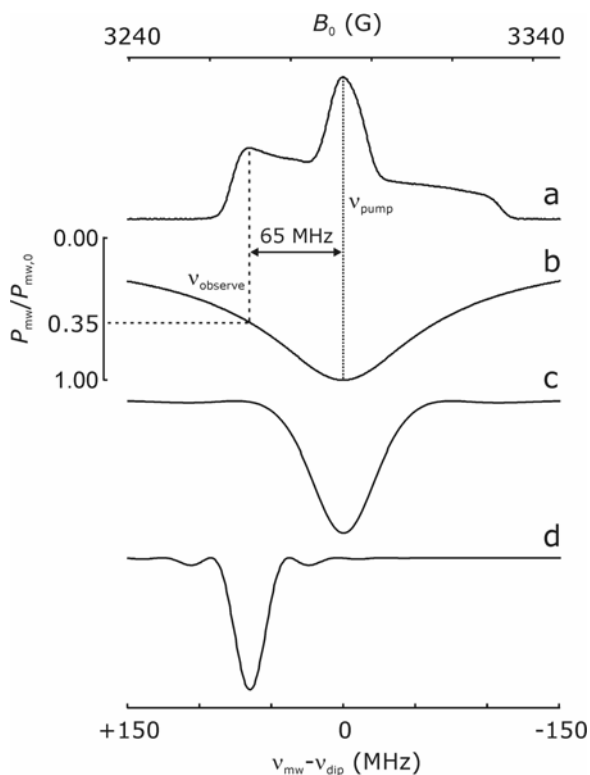
Figure 10. Optimum observer and pump pulse settings in the four-pulse DEER experiment. (a) Echo-detected field-swept ESR spectrum of a nitroxide biradical with a spin-to-spin distance of 5 nm (field ordinate). (b) Simulated idealized m.w. mode assuming $Q_L = 100$ (frequency ordinate power abscissa). (c) Simulated excitation profile of a pump pulse with a length of 12 ns and rise and fall times of 4 ns. (d) Simulated excitation profile of an observer π pulse with a length of 32 ns and rise and fall times of 4 ns.

We now consider what excitation bandwidth of the pulses is required to optimize the sensitivity of pulsed ELDOR distance measurements. This sensitivity depends on the total amplitude of the observed echo and on the fraction of pumped spins, which determines the modulation depth. In the absence of phase noise, the signal-to-noise ratio in the wanted signal is proportional to the product of amplitude and depth. Phase noise is proportional to the echo amplitude; hence, in its presence increasing the modulation depth helps, but increasing echo amplitude

does not. Similarly, the ratio of electron–electron modulation to (unwanted) nuclear modulation depends on modulation depth, but not on total echo amplitude. Hence, increasing the modulation depth is more advantageous than increasing the observer echo amplitude. It follows that the pump pulse at frequency ν_2 (for the pulse sequence, see Figure 7c) should be applied at the maximum of the absorption spectrum and should have the maximum excitation bandwidth that is possible without causing a strong overlap with the excitation band of the observer pulses (Figure 10). We found that a pump pulse with a length of 12 ns (for the excitation profile, see Figure 10c) and observer pulses with a pulse length of 32 ns (Figure 10d) can be applied if the frequency difference is 60 MHz or larger (see Eq. (9)). These conditions are well suited for nitroxides at the X band, as the local maximum at the low-field edge of the absorption spectrum and the global maximum at the center are 60–70 MHz apart (Figure 10a). A good pulse ELDOR setup for nitroxide work should thus allow for π pulses as short as 12 ns. For work on transition metal centers, even shorter pump pulses (and larger frequency differences) would be favorable. With a standard TWT amplifier (1-kW power), 12-ns π pulses can be created, for instance, in a fully overcoupled ($Q_L \approx 100$) Bruker 3 mm split-ring resonator. Loop-gap resonators that fit 0.9 mm tubes or TPX™ (poly(4-methylpentene-1)) capillaries allow for 8-ns π pulses even in the wings of the mode, but are more difficult to handle at low temperatures and may be more difficult to overcouple to very low Q_L.

Strong overcoupling is needed at X-band frequencies to sufficiently broaden the m.w. mode to fit both frequencies (Figure 10b). At W-band or higher frequencies, a critically coupled mode may have a sufficient bandwidth (see Eq. (4)), in particular, since the excitation bandwidths at full m.w. power tend to be lower, so that a smaller difference between pump and observer frequency is feasible.

Any ELDOR experiment that can be performed with two frequencies can in principle also be performed with field-step techniques (Schweiger and Jeschke 2001). In this case all pulses can be applied at the center of the m.w. mode. Our own experience suggests that field-step setups are more difficult to handle in practice. There are two problems. First, to apply a field step, electron coherence has to be stored as polarization and later be reconverted to coherence. During this process inevitably half of the magnetization is lost. Second, to avoid signal distortions the additional field has to decay to a very low and very reproducible value before detection. This introduces an additional waiting time, during which spectral diffusion and spin diffusion may alter the polarization pattern and thus lead to further signal decay or even to spurious frequencies. These problems tend to overcompensate the advantage of complete excitation and detection at the center of the mode.

4.2. Setting up Four-Pulse DEER

To extract reliable distance distributions and to obtain reproducible modulation depths, the four-pulse DEER experiment has to be set up very precisely. Set up starts with measurement of an echo-detected field-swept ESR spectrum (see §2.3)

and selection of the magnetic field at which the pump pulses should be applied (global maximum of the absorption spectrum as in Figure 10a, unless there is a particular reason to pump elsewhere). The pump frequency ν_2 is then set to coincide with the spectrometer frequency ν_1. Next the flip angle of the pump pulse is adjusted, using the inverted-echo sequence $\beta(t_{pump}, \nu_2)-T-\pi/2(t_{observe}/2, \nu_1)-\tau-\pi(t_{observe}, \nu_1)-\tau$ *echo*. The inverted-echo sequence is used for two reasons. First, the pump frequency is not coherent with the reference frequency of the mixer; hence, a usual echo at the pump frequency would have a different phase in each shot and average to zero. Second, the pump pulse indeed has to be optimized for maximum inversion over its whole excitation bandwidth rather than for echo formation. For broad lines, the required flip angle β differs from π and depends on the line shape. For an infinitely broad line, simulations indicate $\beta \approx 3\pi/4$, while for an infinitely narrow line $\beta = \pi$.

For nitroxides, setup of the pump pulse at the X band works well with $t_{pump} = 12$ ns, $t_{observe} = 32$ ns, $T = 400$ ns, and $\tau = 200$ ns. The power of the pump channel is slowly increased until the echo exhibits maximum inversion. Usually this step is done with the pump (and spectrometer) frequencies coinciding with the center of the m.w. mode.

After adjusting pump pulse power, the pump frequency ν_2 is kept fixed. The spectrometer frequency ν_1 is changed by $\Delta\nu = -2.8$ MHz/G $\cdot g/g_e \cdot \Delta B_0$, where ΔB_0 is the difference between the observer and pump position in the field-swept ESR spectrum. For nitroxides, it is sufficiently precise to approximate $g \approx g_e$. We use $\Delta B_0 \approx -23$ G, so that the frequency has to be *increased* by $\Delta\nu \approx 65$ MHz. Then the power and phase of the observer π pulse ($+\langle x \rangle$ channel) are adjusted with a sequence $\pi/2(t_{observe}/2, \nu_1)-\tau-\pi(t_{observe}, \nu_1)-\tau$ *echo*, using the channel attenuator for the power adjustment but the main signal phase shifter for phase adjustment. The observer $\pi/2$ pulse is phase cycled in DEER to eliminate receiver offsets. Hence, the $+x$ and $-x$ channels have to be set using the sequence $\pi/2(t_{observe}, \nu_1)-\tau-\pi(2*t_{observe}, \nu_1)-\tau$–*echo* and the *channel* phase shifters. After that, a standing DEER experiment $\pi/2(t_{observe}, \nu_1)-\tau_1-\pi(t_{observe}, \nu_1)-\tau_1-\beta(t_{pump}, \nu_2)-\tau_2-\pi(t_{observe}, \nu_1)-\tau_2$–*echo* (as in Figure 7c, but with $t = 0$) is used to readjust the *signal* phase (main phase shifter). This adjustment is initially best done with $\tau_1 = 200$ ns and $\tau_2 = 800$ ns. If the solvent or the spin label is deuterated, $\tau_1 = 400$ ns is a better choice. Selection of the τ_2 value for the actual DEER measurement depends on the expected distances. A detailed discussion and a description of variable-time DEER as a technique for sensitivity enhancement are given by Jeschke et al. (2004a).

4.3. Relations between Setup and Data Analysis

Software for data analysis is available at http://www.mpip-mainz.mpg.de/ ~jeschke/distance.html and is also included with the accompanying CD-ROM of this book. The software package includes a manual. Using this software, distance distributions $P(r)$ can be extracted from pulsed ELDOR data. This corresponds to a moderately ill-posed problem (Jeschke et al. 2002) that can be considerably stabilized by implementing the constraint $P(r) > 0$ (Jeschke et al. 2004b). Yet to main-

tain stability it is of utmost importance that as few parameters as possible need to be fitted, that systematic differences between the theoretically expected and experimentally observed dipolar evolution function are as small as possible, and that the signal-to-noise ratio is as high as possible. Minimization of the number of fit parameters requires that the signal can be normalized. For this the maximum at dipolar evolution time zero and the zero level at infinite dipolar evolution time have to be known. To know the maximum the experiment must be free of dead time. The zero level is not exactly known as the detector may have a small offset. To eliminate this receiver offset completely, the observer $\pi/2$ pulse is phase cycled $+x/-x$ and the two signals subtracted.

Systematic differences between the theoretically expected and experimentally observed dipolar evolution functions are mainly due to nuclear modulation and orientation selection. The depth of the dipolar modulation can be optimized with respect to the depth of nuclear modulations by using the largest feasible excitation bandwidth for the pump pulses and by adjusting pump pulse power to complete inversion. Nuclear modulations can be partially averaged by varying τ_1 in 8 steps of 8 ns and adding the signals. Orientation selection cannot generally be avoided. As it is less dramatic at lower fields, distance measurements should be performed at high fields only if there is a good reason to do so or if orientation selection is intended. To check experimentally for orientation selection effects, pump and observer positions have to be varied. The signal-to-noise ratio is optimized by careful adjustment of the phase and power of all channels, and in many cases by applying the variable-time DEER experiment (Jeschke et al. 2004a).

Another frequently encountered problem during long measurements is the phase drift of the signal. It is therefore advisable to adjust the phase carefully with the standing DEER experiment before starting the measurement and to use quadrature detection. That way phase drifts can be recognized and small drifts can be compensated by a phase correction of the whole signal trace after the measurement. A large phase drift ($>10°$) points to stability problems of the spectrometer that should be solved.

With proper setup procedures, modulation depths for the same sample should be reproducible to within less then 2% of the total signal. Modulation depth scaled signals of the same sample should differ only by white noise.

5. ACKNOWLEDGMENTS

6. PROBLEMS

P0. Sample Preparation

The two experimental problems are based on standard samples for measurements at room temperature that can be prepared easily: ground coffee. Strongly roasted varieties give a somewhat stronger signal. Answers to the problems were prepared with Cafét Siesta (100% Arabica, available from the German supermarket chain Penny Market). Line width, radical concentration, and relaxation times may differ for other brands of coffee. Coffee is a sample with a signal of comparable strength to spin-labeled membrane proteins. The same experiments can be performed with less averaging, i.e., in a shorter time with a coal sample. For instance, the coal standard sample that comes with a Bruker pulsed ESR spectrometer is suitable as well.

P1. Optimization of CW ESR Conditions

Find the maximum m.w. power (minimum attenuation) and maximum modulation depth that can be used for measuring an undistorted CW ESR line shape for the coffee sample.

P2. Echo Integration in Field-Swept ESR

Measure the echo-detected field-swept ESR spectrum of coffee with a sequence $\pi/2$(16 ns)–delay(200 ns)–π(32 ns)–delay–*echo* (a) with an integration window length t_{intg} = 200 ns, and (b) with t_{intg} = 32 ns. Compare signal-to-noise ratio and line shape.

P3. Choice of Resonator

Assume that you want to make a pulsed ELDOR distance measurement at the X band (9.6 GHz) between an organic radical and a metal center ($S = 1/2$, g = 2.1) for which you expect to need a resonator bandwidth of 500 MHz and pump pulses with a flip angle of $3\pi/4$ and a length of 8 ns. Allowing for losses in the transmission line and circulator, the incident m.w. power at your resonator is 200 W. Estimate the effective volume of a resonator that would allow for such an experiment.

7. ANSWERS

A1. Optimization of CW ESR Conditions

For Cofét Siesta, signal intensity increases with less than the square root of the m.w. power for P_{mw} > mW, i.e., 40-dB attenuation on a Bruker Elexsys 580 spectrometer (see Figure 11). The line width at 40 dB attenuation, measured with a modulation amplitude of 1 G, is 11 G. Hence, an undistorted line shape can be measured with maximum sensitivity at 40-dB attenuation and 2-G modulation amplitude. Note that values may differ somewhat for other brands of coffee.
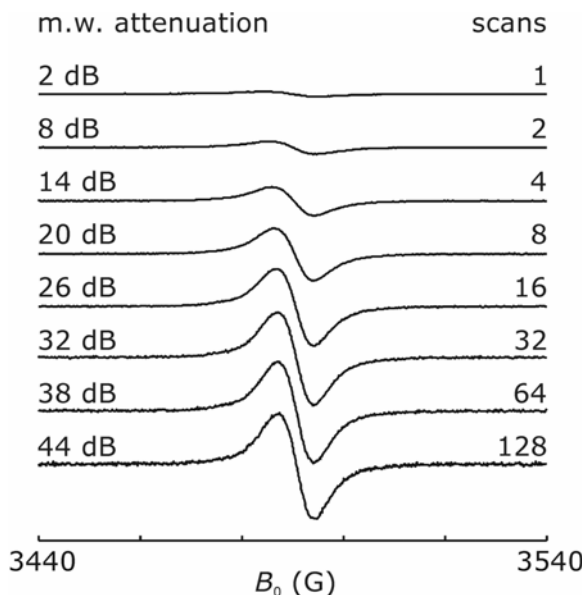
Figure 11. CW ESR measurements with different m.w. power level on a coffee sample. In the absence of saturation, all spectra should have the same amplitude.

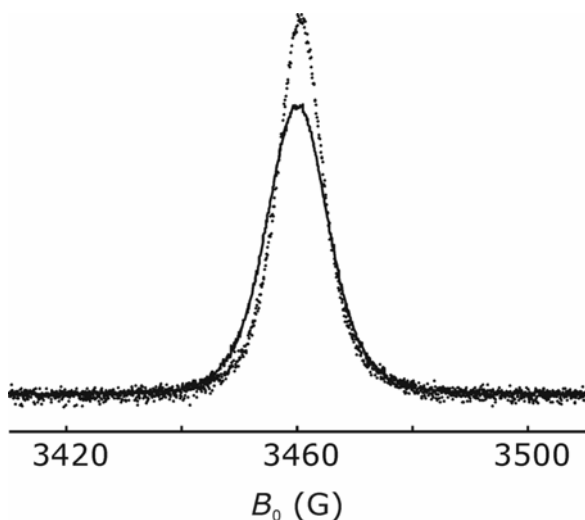## A2. Echo Integration in Field-Swept ESR

Typical results are shown in Figure 12. The signal-to-noise ratio is significantly better with the 32-ns window, but the line is also significantly broadened.

A3. Choice of Resonator

$Q_L = \nu_{mw}/\Delta\nu = 19.2$. $B_1 = \beta h/(2\pi g\mu_B t_p) = 1.6 \cdot 10^{-3}$ T. $V_C = 2\mu_0 \, Q_L \, P_{mw}/(\nu_{mw} B_1^2) = 392$ mm^3 = 392 μL. Note, however, that the sample volume is much smaller.

8. REFERENCES

Bietsch W, von Schütz JU. 1993. ???full cite: article title???. *Bruker Report* **139**:12.

Borbat PP, Freed JH. 2000. Double quantum ESR and distance measurements. In *Distance measurements in biological systems by EPR*, pp. 383–459. Ed L Berliner, SS Eaton, GR Eaton. New York: Kluwer.

Burghaus O, Rohrer M, Götzinger T, Plato M, Möbius K. 1992. A novel high-field high-frequency EPR and ENDOR spectrometer operating at 3 mm wavelength. *Meas Sci Technol* **3**:765–774.

Davies ER. 1974. New pulse ENDOR technique. *Phys Lett* **A47**:1–2.

Figure 12. Echo-detected field-swept EPR on a coffee sample with integration gate widths of 32 (solid line) and 200 ns (dots). Amplitudes have been scaled so that the integral of the absorption spectrum is the same for both cases.

Epel B, Arieli D, Baute D, Goldfarb D. 2003. Improving W-band pulsed ENDOR sensitivity: acquisition and pulsed special TRIPLE. *J Magn Reson* **164**:78–83.

Feher G. 1957. Sensitivity considerations in microwave paramagnetic resonance absorption techniques. *Bell Syst Techol J* **36**:449–484.

Forrer J, Pfenninger S, Eisenegger J, Schweiger A. 1990. A pulsed ENDOR probehead with the bridged loop-gap resonator: construction and performance. *Rev Sci Instrum* **61**:3360–3367.

Froncisz, W, Hyde JS. 1982. The loop-gap resonator: a new microwave lumped circuit electron-spin-resonance sample structure. *J Magn Reson* **47**:515–521.

Gemperle C, Schweiger A. 1991. Pulsed electron-nuclear double resonance methodology. *Chem Rev* **91**:1481–1505.

Höfer P, Grupp A, Nebenführ H, Mehring M. 1986. Hyperfine sublevel correlation (HYSCORE) spectroscopy: a 2D electron-spin-resonance investigation of the squaric acid radical. *Chem Phys Lett* **132**:279–282.

Jeschke G, Pannier M, Godt A, Spiess HW. 2000. Dipolar spectroscopy and spin alignment in electron paramagnetic resonance. *Chem Phys Lett* **331**:243–252.

Jeschke G, Koch A, Jonas U, Godt A. 2002. Direct conversion of EPR dipolar time evolution data to distance distributions. *J Magn Reson* **155**:72–82.

Jeschke G, Bender A, Paulsen H, Zimmermann H, Godt A. 2004a. Sensitivity enhancement in pulse EPR distance measurements. *J Magn Reson* **169**:1–12.

Jeschke G, Panek G, Godt A, Bender A, Paulsen H. 2004b. Data analysis procedures for pulse ELDOR measurements of broad distance distributions. *Appl Magn Reson* **26**:223–244.

Milov AD, Ponomarev AB, Tsvetkov YuD. 1984. Electron–electron double resonance in electron spin echo: model biradical systems and the sensitized photolysis of decalin. *Chem Phys Lett* **110**:67–72.

Milov AD, Maryasov AG, Tsvetkov YuD. 1998. Pulsed electron double resonance (PELDOR) and its application in free-radicals research. *Appl Magn Reson* **15**:107–143.

Mims WB. 1965. Pulsed ENDOR experiments. *Proc Roy Soc London* **A283**:452–457.

Pannier M, Veit S, Godt A, Jeschke G, Spiess HW. 2000. Dead-time free measurement of dipole-dipole interactions between electron spins. *J Magn Reson* **142**:331–340.

Pfenninger S, Forrer J, Schweiger A, Weiland T. 1988. Bridged loop gap resonator: a resonant structure for pulsed electron-spin-resonance transparent to high-frequency radiation. *Rev Sci Instrum* **59**:752–760.

Poole ChP. 1997. Electron paramagnetic resonance (a comprehensive treatise on experimental techniques), 2nd ed. New York: Dover.

Rohrer M, Plato M, MacMillan F, Grishin Y, Lubitz W, Möbius K. 1995. Orientation-selected 95 GHz high-field ENDOR spectroscopy of randomly oriented plastoquinone anion-radicals. *J Magn Reson* **A116**:59–66.

Schweiger A, Jeschke G. 2001. Principles of pulse electron paramagnetic resonance. Oxford: Oxford UP.

Schweiger A, Gemperle C, Ernst RR. 1990. Soft pulse electron-spin-echo-envelope modulation spectroscopy (Soft ESEEM). *J Magn Reson* **86**:70–81.

Weil JA, Bolton JR, Wertz JE. 1994. *Electron paramagnetic resonance*. New York: Wiley.

Zänker PP, Jeschke G, Goldfarb D. 2004. Distance measurements between paramagnetic centers and a planar object by matrix Mims ENDOR. *J Chem Phys* **122**, 024515-11.